Acta Crystallographica Section B
Structural Science
ISSN 0108-7681

Structure of an aluminophosphate EMM-8: a multi-technique approach

Guang Cao, Mobae Afeworki, Gordon J. Kennedy, Karl G. Strohmaier and Douglas L. Dorset*

Corporate Strategic Research, ExxonMobil Research and Engineering Company, Clinton, NJ 08801, USA

Correspondence e-mail: d.l.dorset@exxonmobil.com

Received 27 July 2006
Accepted 29 September 2006

The crystal structure of an aluminophosphate, EMM-8 (ExxonMobil Material #8), was determined in its calcined, anhydrous form from synchrotron powder diffraction data using the computer program *FOCUS*. A linkage of double four-ring (D4R) building units forms a two-dimensional framework with 12-MR and 8-MR channels, and differs from a similar SAPO-40 (**AFR**) framework only by the relationship between paired D4R units. Rietveld refinement reveals a fit of the model to the observed synchrotron data by $R_{wp} = 0.1118$, $R(F^2) = 0.1769$. Local environments of the tetrahedral phosphorus and aluminium sites were established by solid-state NMR, which detects distinct differences between as-synthesized and calcined materials. Distinct, reversible changes in the local symmetry of the P and Al atoms were observed by NMR upon calcination and subsequent hydration. These NMR data provided important constraints on the number of tetrahedral (T) atoms per unit cell and the connectivities of the T atoms. Detailed local structural information obtained by solid-state NMR thereby guided the ultimate determination of the structure of AlPO EMM-8 from the powder data. Comparisons are made to the recently published crystal structure of the fluoride-containing, as-synthesized SSZ-51, indicating that the unit-cell symmetry, axial dimensions and framework structure are preserved after calcination.

1. Introduction

Microporous materials, including zeolites and silicoaluminophosphates, are widely used in the petroleum industry as absorbents, catalysts and catalyst supports. Their crystalline structures consist of three-dimensional frameworks containing uniform pore openings, channels and internal cages of dimensions (< 20 Å) similar to most hydrocarbons. The composition of the frameworks can be such that they are anionic, which requires the presence of non-framework cations to balance the negative charge. These non-framework cations are exchangeable and, if converted to the proton form, impart Brønsted acid sites to the material having catalytic activity. The combination of acidity and restricted pore openings gives these materials catalytic properties which are not available for other materials because of their ability to exclude or restrict some of the products, reactants and/or transition states in many reactions. Non-reactive materials, such as pure silica and aluminophosphate frameworks are also useful and can be used in the adsorption and separation processes of liquids, gases and reactive molecules such as alkenes.

The family of crystalline microporous materials known as molecular sieves, which exhibit the ion-exchange and/or adsorption characteristics of zeolites, comprises the aluminophosphates, identified by the acronym AlPO (Wilson *et al.*, 1982), silicon-substituted aluminophosphates or silicoaluminophosphates, identified by the acronym SAPO (Lok *et al.*, 1984), and metal-substituted aluminophosphates, identified by the acronym MeAPO (Me = metal). AlPOs, SAPOs and MeAPOs have different structures, as identified by their X-ray diffraction patterns, and are designated by a number after AlPO, SAPO, MeAPO (Lok *et al.*, 1984).

In the petroleum industry, microporous materials, such as faujasite, mordenite and ZSM-5, are extensively employed in many commercial applications, such as reforming, cracking, hydrocracking, alkylation, oligomerization, dewaxing and isomerization of hydrocarbons (Corma, 2003). Any new material has the potential to improve the catalytic performance over those catalysts presently employed. There are currently over 165 known microporous framework structures as tabulated by the International Zeolite Association (IZA; Baerlocher *et al.*, 2001). Each structure has unique pore, channel and cage dimensions, which characterize its particular properties as described above. In this report we describe the structural characterization and structure of the new crystalline, microporous aluminophosphate material EMM-8. As explained in a classic review (McCusker, 1991) and illustrated in this report, a reliable structure analysis, based on data from microporous samples, requires the consensus of various techniques in order to validate a proposed structural model. Comparisons are made to the crystal structure (based on single-crystal X-ray data) of an as-synthesized precursor, SSZ-51 (IZA framework code **SFO**), that contains fluoride (Morris *et al.*, 2004).

2. Materials and methods

2.1. Materials

The structure-directing agent (SDA) employed in the synthesis of EMM-8 was *N*,*N*-dimethylamino-4-pyridine (DMAPy). $AlPO_4$–EMM-8 can be prepared with either of the two gel compositions:

(i) 2.0 DMAPy:1.0 Al_2O_3:1.0 P_2O_5:40 H_2O;

(ii) 0.5 HF: 2.0 DMAPy: 1.0 Al_2O_3: 1.0 P_2O_5: 40 H_2O.

Crystallization was carried out at 453 K for 2–4 d. SAPO–EMM-8 was prepared without fluoride and with the addition of 0.1–0.7 mol SiO_2 per mol of Al_2O_3 in the gel. Therefore, EMM-8 could be made as both $AlPO_4$ and SAPO, and the SAPO was found to have typical solid acid properties such as catalytic activity in the cracking of hydrocarbons. Adsorption data with test molecules indicated that the material has a large adsorption capacity and pore openings delineated by at least a 12-ring. Calcination in air was carried out at 723 K for 3 h.

2.2. Powder X-ray diffraction

Debye–Scherrer X-ray diffraction measurements on calcined, anhydrous EMM-8 in its $AlPO_4$ form, in 1 mm diameter capillaries, were obtained at the ExxonMobil beamline X10B at the Brookhaven National Laboratory (λ = 0.86780 Å), and also on a laboratory instrument with Cu $K\alpha$ radiation. In addition to single-crystal electron diffraction evaluations (see below), patterns were also indexed with the *JADE* software package from MDI, Inc. (Materials Data Inc., 2005). The crystal structure was solved using the direct-methods software package *FOCUS* (Grosse-Kunstleve *et al.*, 1999). Rietveld refinements of the structural models were made with *GSAS* (Larson & Von Dreele, 1994). Silicate models used for Rietveld refinement were first refined by distance least squares (DLS; Baerlocher *et al.*, 1977) to optimize bonding parameters.

2.3. Electron diffraction

Transmission electron-diffraction measurements were initially carried out at 300 kV with a Philips/FEI CM30 electron microscope (λ = 0.01968 Å). The aluminophosphate sample was first crushed to a fine powder in a mortar and pestle, and then suspended in acetone in an ultrasonic bath. Drops of the fine particle suspension were then dried on carbon-film-covered 300-mesh copper electron microscope grids. Selected-area electron diffraction patterns were recorded on a Kodak SO-163 electron microscope film developed in a Kodak HRP developer. Reciprocal spacings in diffraction patterns were calibrated against a gold powder standard.

2.4. Multinuclear solid-state NMR

^{27}Al and ^{31}P MAS NMR spectra were recorded on an 11.7 T Varian InfinityPlus 500 spectrometer corresponding to Larmor frequencies of 130 and 202 MHz, respectively. The ^{27}Al MAS NMR spectra were obtained with a $\pi/12$ rad pulse length and a recycle delay of *ca* 0.2 s. The ^{31}P MAS spectra were obtained with a $\pi/4$ rad pulse length and a recycle delay of 300 s. The samples were loaded in 4 mm (o.d.) MAS rotors and spun at the magic angle at rates of 10–16 kHz. All measurements were carried out at room temperature. The ^{27}Al and ^{31}P chemical shifts were referenced with respect to external solutions of $Al(H_2O)_6^{3+}$ (δ_{Al} = 0.0 p.p.m.) and 85% H_3PO_4 (δ_P = 0.0 p.p.m.), respectively.

The solid-state ^{27}Al multiple-quantum (MQ) MAS NMR spectra were recorded using the IP-500 and a Varian triple-resonance 4 mm T3 TR probe. The MQMAS pulse sequence used was 3QMAS with a Z-filter, with parameters similar to those previously reported (Fernandez *et al.*, 1996, 2002; Amoureux & Pruski, 2002). The $^{19}F \rightarrow {}^{27}Al$ CPMAS NMR spectra were recorded on as-synthesized AlPO EMM-8 on a sample loaded in a 3.2 mm rotor spinning at 18 and 12-kHz, respectively.

3. Results

3.1. Crystallographic analyses

Table 1 summarizes the crystallographic data. Several indexings for the laboratory and synchrotron powder data

Table 1
Experimental data.

Crystal data	
Chemical formula	$Al_{32}P_{32}O_{128}$
Cell setting, space group	Monoclinic, *C*2/*c*
Temperature (K)	29 K
a, *b*, *c* (Å)	22.5541 (3), 13.7357 (2), 14.0756 (2)
β (°)	98.6174 (18)
V (Å^3)	4311.35 (9)
Z	32
D_x (Mg m^{-3})	1.503
Radiation type	Synchrotron
Specimen form, color	Lath, colorless
Data collection	
Diffractometer	Brookhaven X10B
Data collection method	Debye–Scherrer powder
2θ (°)	$2\theta_{min}$ = 2.00138, $2\theta_{max}$ = 52.04638, increment = 0.005
Refinement	
Refinement on	Rietveld parameters
R factors and goodness-of-fit	R_p = 0.082, R_{wp} = 0.112, R_{exp} = 0.068, *S* = 1.68
Wavelength of incident radiation (Å)	0.86780
Excluded region(s)	< 3.5°, > 50°
Profile function	CW profile function number 2 with 18 terms†
No. of parameters	17
$(\Delta/\sigma)_{max}$	0.48

Computer programs used: *FOCUS* (Grosse-Kunstleve *et al.*, 1999), *GSAS* (Larson & Von Dreele, 1994). † Profile coefficients for Simpson's rule integration of pseudovoigt function.

were suggested by the program *JADE* (Materials Data Inc., 2005). Such ambiguities are frequently encountered (Morris *et al.*, 2004). Supported by two electron-diffraction zonal patterns, *i.e.* *hk*0, where $h + k = 2n$ and $h0\ell$, where $h = 2n$ (Fig. 1), a monoclinic unit cell was indicated in the space group *C*2, *Cm* or *C*2/*m*. (Owing to multiple scattering perturbations, only the dimensional information could be used and not the spot intensities.) The unit-cell parameters after a LeBail extraction (LeBail *et al.*, 1988) of intensities by *GSAS* (Larson & Von Dreele, 1994), assuming equi-partitioning of the overlaps, were *a* = 22.5554, *b* = 13.7359, *c* = 7.03799 Å, β = 98.615°. (Morris *et al.*, 2004, also observed that calcination and dehydration of SSZ-51 preserves the unit-cell dimensions and the C-centered monoclinic symmetry.) The crystal structure was solved by *FOCUS* (Grosse-Kunstleve *et al.*, 1999), giving a consistent solution with four unique *T* sites only in the space group *C*2/*m*. A DLS refinement of this model resulted in *R* = 0.00399 before the ninth cycle.

Although an all-silicon model provided a good approximate fit to the observed diffraction pattern, a closer look found that there were some weak peaks not accounted for by the assumed unit cell. An aluminophosphate framework was constructed using the *Cerius*^{2} (Accelrys Inc., 1997) model building software. It was soon found that the *c* axis should be doubled in order to yield a consistent interchange of the two *T*-atom site species to avoid violations of Löwenstein's rule (Löwenstein, 1954; Bell *et al.*, 1992). Evaluation of the symmetry of the resultant superlattice construction revealed that the space group *C*2/*c* should be selected, again doubling the *c*-axis value. The resultant model is depicted in Fig. 2.

Rietveld refinement of the framework model with *GSAS* (Larson & Von Dreele, 1994) against the powder data (just completed as the structure of SSZ-51 was published) gives a good fit (Fig. 3), where R_{wp} = 0.1115, $R(F^2)$ = 0.1773. The refined unit-cell dimensions are: *a* = 22.5541 (3), *b* = 13.7357 (2), *c* = 14.0756 (2) Å, β = 98.618 (2)°. Final atomic coordinates have been deposited.[1] The *T*-site positions are, on average, within 0.27 Å of those identified for the SSZ-51 model (Morris *et al.*, 2004). Bond distances and angles are listed in Table 2. The average bond distances found were d_{Al-O} = 1.69 (3), d_{P-O} = 1.58 (3) Å and average bond angles O—Al—O 109 (4), O—P—O 109 (4), Al—O—P 143 (6)°. The first two bond angles through the *T* atoms should be compared with the ideal tetrahedral angle and the latter angle through linkage O atoms to an expected value of 145°. From the single-crystal study of SSZ-51 (Morris *et al.*, 2004), d_{Al-O} = 1.76 (3), d_{P-O} = 1.53 (1) Å. For the penta-coordinate Al sites, there are two long Al—O bonds (1.81 and 1.84 Å). The average O—P—O angle for SSZ-51 is 109 (1)°, which is similar to EMM-8, but the average O—Al—O angle is 108 (10)°, revealing distortions from tetrahedral geometry due to the fluoride linkage. The coordination sequence (Meier & Moeck, 1979) and vertex symbols (O'Keeffe & Hyde, 1997) for *T* sites are given in Table 3 and are duplicated for the Al and P positions, respectively. We find identical values using the published coordinates for SSZ-51 (Morris *et al.*, 2004), verifying that both structures share a common framework geometry. The final *T*-site density is 15.0 T per 1000 Å^3.

3.2. NMR analyses

Fig. 4 shows the 11.7*T* ^{27}Al (left) and ^{31}P (right) MAS NMR spectra of the as-synthesized and calcined AlPO EMM-8. These data show that the Al in the as-synthesized sample is present in multiple tetrahedral and penta-coordinated environments. The tetrahedral peak(s) are centered around 40 p.p.m. and penta-coordinated peak(s) are centered around 20 p.p.m. in an intensity ratio of approximately 1:1. All the Al becomes tetrahedral upon calcination and drying. The ^{31}P MAS spectrum of the as-synthesized AlPO EMM-8 material shows three major resonances in the ratio of 2:1:1, suggesting at least three crystallographically distinct sites. Two resonances in a 1:1 ratio are observed in the calcined AlPO EMM-8 material. (Similar observations were made by Morris *et al.*, 2004.) The calcination-induced changes in these spectra are a reflection of the structural changes that occur upon removal of the structure directing agent (SDA) and the fluoride ions from the framework. Calcination results in a completely tetrahedral framework.

It is likely that one or more of the penta-coordinated Al peaks identified in Fig. 4 is due to the interaction of F with the framework. Unambiguous assignment is not possible on the

[1] Supplementary data for this paper are available from the IUCr electronic archives (Reference: WS5052). Services for accessing these data are described at the back of the journal.

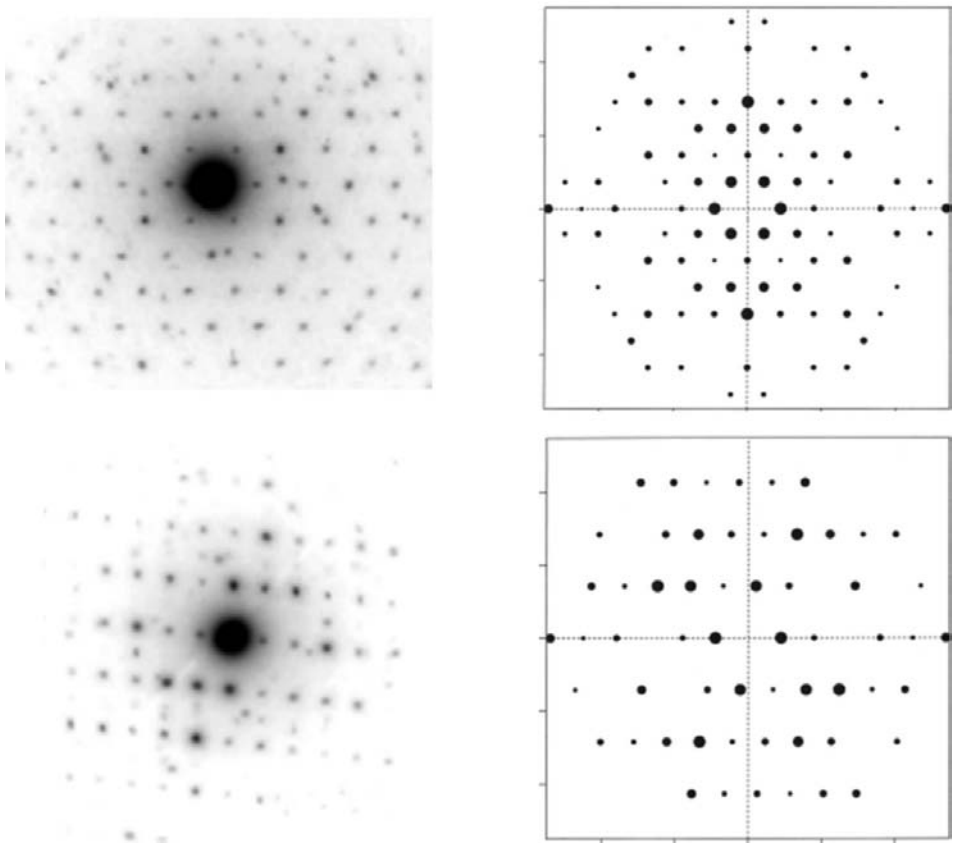

Figure 1
Comparison of experimental (left) and simulated (right) electron diffraction patterns from EMM-8; top: $hk0$, bottom $h0\ell$.

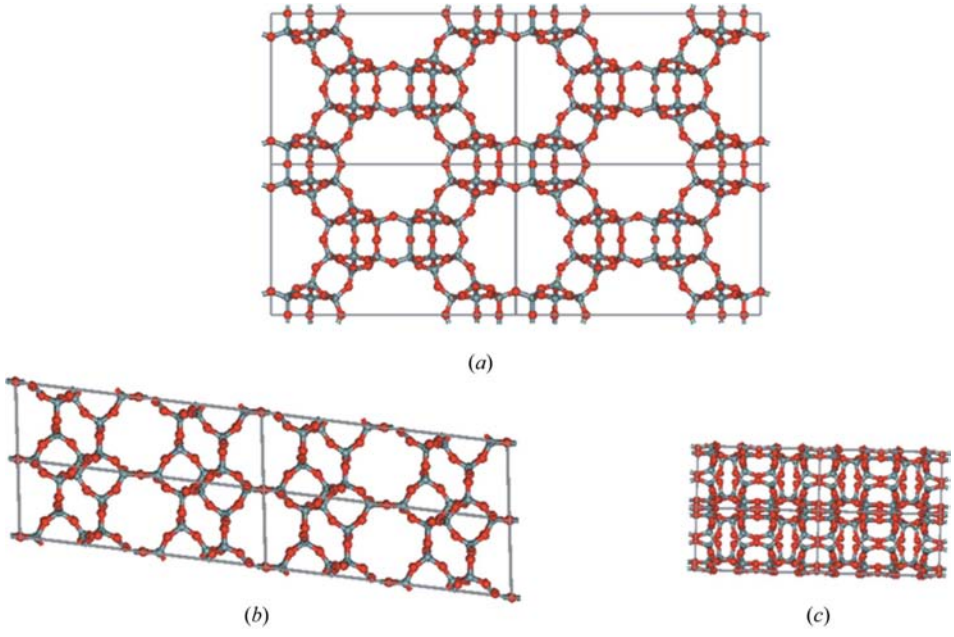

Figure 2
Underlying framework structure of EMM-8, projected down: (*a*) [001]; (*b*) [010]; (*c*) [100].

basis of chemical shift alone. However, with $^{19}F \rightarrow {}^{27}Al$ CPMAS NMR it is possible *via* some spectral editing to identify the Al species that interact with F. The $^{19}F \rightarrow {}^{27}Al$ CPMAS NMR spectra (not shown) clearly show that *only* the penta-coordinated Al species directly interacts with the fluoride species; the T_d ($T_d \equiv$ Schoenflies point group) species do not cross-polarize, indicating that they are further away. Furthermore, the penta-coordinated species obtained from the ^{19}F-to-^{27}Al CPMAS appears to be narrower than that obtained by ^{27}Al MAS NMR and this appears to indicate that the two penta-coordinated species (obtained by 3QMAS) may have different distances to the F species. The X-ray structure of SSZ-51 (Morris *et al.*, 2004) reveals a slight difference (0.5 Å) between the Al—F bond distances.

3.3. ^{27}Al 3QMAS NMR: multiple crystallographic sites in AlPO and SAPO EMM-8

The ^{27}Al MAS spectra of AlPO EMM-8 (Fig. 4) showed asymmetric tetrahedral and penta-coordinated peaks for the as-synthesized form and asymmetric tetrahedral peaks for the calcined form. The multiple resonances in these ^{27}Al MAS NMR spectra are likely due to a combination of crystallographically distinct sites and non-averaged second-order quadrupolar broadening. Since ^{27}Al is a quadrupolar nucleus, MAS alone does not completely average the residual second-order quadrupolar interaction. Multiple quantum MAS (MQMAS) techniques are two-dimensional MAS NMR experiments that remove this residual quadrupolar broadening. That is, the isotropic spectrum (*i.e.* free from quadrupolar broadening) is observed in the second dimension of an MQMAS data set. Fig. 5 shows the 130.07 MHz (11.7 T) 3QMAS NMR spectra of as-synthesized (*A*) and calcined (*B*) AlPO EMM-8.

Table 2
Bond distances (Å) and angles (°) for refined EMM-8.

Al1—O9	1.70 (2)	O9—Al1—O13	108.5 (16)	O9—P5—O10	105.9 (18)
Al1—O13	1.67 (2)	O9—Al1—O14	112.6 (18)	O9—P5—O12	109.3 (18)
Al1—O14	1.67 (2)	O9—Al1—O15	108.4 (17)	O9—P5—O21	107.0 (17)
Al1—O15	1.73 (2)	O13—Al1—O14	109.4 (18)	O10—P5—O12	105.3 (17)
Al2—O11	1.68 (2)	O13—Al1—O15	110.6 (17)	O10—P5—O21	111.9 (19)
Al2—O19	1.67 (2)	O14—Al1—O15	107.4 (17)	O12—P5—O21	116.9 (18)
Al2—O20	1.69 (2)	O11—Al2—O19	109.2 (17)	O13—P6—O16	109.3 (17)
Al2—O22	1.67 (2)	O11—Al2—O20	108.7 (18)	O13—P6—O18	107.1 (19)
Al3—O10	1.72 (2)	O11—Al2—O22	115.8 (18)	O13—P6—O20	108.0 (18)
Al3—O16	1.66 (2)	O19—Al2—O20	110.2 (18)	O16—P6—O18	114.3 (16)
Al3—O18	1.70 (2)	O19—Al2—O22	109.9 (17)	O16—P6—O20	113.1 (17)
Al3—O23	1.73 (2)	O20—Al2—O22	102.8 (16)	O18—P6—O20	104.7 (17)
Al4—O12	1.72 (2)	O10—Al3—O16	111.0 (17)	O11—P7—O14	108.3 (17)
Al4—O17	1.68 (2)	O10—Al3—O18	106.6 (17)	O11—P7—O17	107.0 (16)
Al4—O21	1.75 (2)	O10—Al3—O23	105.5 (17)	O11—P7—O22	111.6 (18)
Al4—O24	1.62 (2)	O16—Al3—O18	114.0 (16)	O14—P7—O17	113.3 (17)
P5—O9	1.58 (2)	O16—Al3—O23	110.7 (17)	O14—P7—O22	112.1 (18)
P5—O10	1.57 (2)	O18—Al3—O23	108.6 (18)	O17—P7—O22	104.4 (16)
P5—O11	1.56 (2)	O12—Al4—O17	105.1 (15)	O15—P8—O19	105.8 (18)
P5—O21	1.56 (2)	O12—Al4—O21	107.1 (17)	O15—P8—O23	113.7 (19)
P6—O13	1.61 (2)	O12—Al4—O24	108.3 (17)	O15—P8—O24	113.7 (17)
P6—O16	1.53 (2)	O17—Al4—O21	107.8 (16)	O19—P8—O23	106.8 (17)
P6—O18	1.59 (2)	O17—Al4—O24	120.5 (17)	O19—P8—O24	109.4 (17)
P6—O20	1.60 (2)	O21—Al4—O24	107.3 (17)	O23—P8—O24	107.2 (19)
P7—O11	1.62 (2)	Al1—O9—P5	150.3 (22)	Al4—O17—P7	135.2 (11)
P7—O14	1.54 (2)	Al3—O10—P5	142.0 (24)	Al3—O18—P6	141.2 (11)
P7—O17	1.58 (2)	Al2—O11—P7	138.6 (22)	Al2—O19—P8	149.2 (22)
P7—O22	1.60 (2)	Al4—O12—P5	135.5 (23)	Al2—O20—P6	140.2 (23)
P8—O15	1.58 (2)	Al1—O13—P6	144.2 (23)	Al4—O21—P5	139.0 (21)
P8—O19	1.61 (2)	Al1—O14—P7	153.4 (23)	Al2—O22—P7	136.8 (24)
P8—O23	1.54 (2)	Al1—O15—P8	138.1 (12)	Al3—O23—P8	144.9 (23)
P8—O24	1.58 (2)	Al3—O16—P6	149.5 (13)	Al4—O24—P8	145.6 (22)

Table 3
T-site coordination sequence vertex symbols.

The sequence can be found for equivalent Al and P atoms (Al2, Al3, Al4, Al1; P5, P6, P7, P8).

T site	Coordination sequence	Vertex symbols
*T*1	4 10 17 28 46 63 86 117 142 168	4 6 4 6 6 12
*T*2	4 9 18 30 43 64 90 111 139 178	4 4 4 4 8 6_3 8
*T*3	4 9 18 29 42 65 91 111 138 176	4 4 4 12 6 6_3
*T*4	4 9 16 27 44 65 87 110 138 171	4 6 4 6_2 4 8

The projections of the two dimensions are shown on the two-dimensional plot. The vertical projection (x axis) shows the MAS spectrum and is complicated by the non-averaged quadrupolar broadening. The horizontal projection shows the isotropic spectrum. The 3QMAS spectrum of the as-synthesized form clearly shows at least two tetrahedral sites ($\delta \simeq 45$–30 p.p.m. region) and two penta-coordinated sites ($\delta \simeq 20$ p.p.m.). Similarly, the 3QMAS spectrum of the calcined form clearly shows at least two tetrahedral sites ($\delta \simeq 40$–30 p.p.m. region). This confirms that ^{27}Al MAS NMR spectra are complicated by residual quadrupolar broadening, making spectral interpretation ambiguous. The breadth and symmetry of the contours in each two-dimensional plot qualitatively indicate the size and asymmetry of the quadrupole coupling constant for each crystallographic *T* site.

4. Discussion

In the earliest structure determination of SAPO-40 (Estermann *et al.*, 1992), it was noted that 65% of the reflections were overlapped in the powder diffraction pattern owing to the approximate framework relationships ($a = 22.045$, $b = 13.699$, $c = 7.120$ Å, space group *Pmmn*) $a \simeq 3c$ and $b \simeq 2c$. This overlap made structure determination by conventional direct methods very difficult. A similar problem would therefore occur for EMM-8 and demonstrates the power of *FOCUS* (Grosse-Kunstleve *et al.*, 1999) to solve structures from powder data in such cases. A review discussing how *FOCUS* has become an invaluable tool for determining zeoform structures from powder diffraction data has appeared recently (Burton, 2004).

The framework structure is built from a so-called 'ring-opened' D4R unit, linked head-to-tail to form chains along the *c*-axis direction. It results in a projected 12-MR channel parallel to [001] and an 8-MR channel parallel to [010]. The structure is remarkably similar to that of SAPO-40 (**AFR**; Estermann *et al.*, 1992; Dumont *et al.*, 1993; McCusker & Baerlocher, 1996), that comprises the same building unit as well as the projected straight channels of the same dimension. (Pictorial representations of these structural differences, explaining the shift from orthorhombic to monoclinic unit cells, are found in the paper by Morris *et al.*, 2004.) By coincidence, owing to the close similarity of unit-cell dimensions, the **AFR** framework had been selected to model the *T*-site density. Also, it is clear that, like EMM-8, the framework symmetry for **AFR**, *Pmmn*, is different from that of SAPO-40, *Pccn*, requiring the *c* axis to be doubled owing to the interchange of Si, Al and P sites. Comparison of EMM-8 to SAPO-40 demonstrates that the former monoclinic structure is formed when the four-ring bridge between D4R building units involves a center of inversion, whereas the latter is formed when these units are related by a mirror. Similar relationships have been found for other microporous materials, *e.g.* ITQ-3 (**ITE**) *versus* RUB-13 (**RTH**), as discussed by Wagner *et al.* (2000).

Several important conclusions regarding the structure of EMM-8 can be drawn from the NMR study. ^{31}P MAS NMR spectroscopy shows that there are at least three distinct environments for the P atoms in the as-synthesized AlPO EMM-8 in a ratio of 2:1:1, and a minimum of two in the ratio 1:1 in the calcined material. ^{27}Al MAS NMR shows tetra-

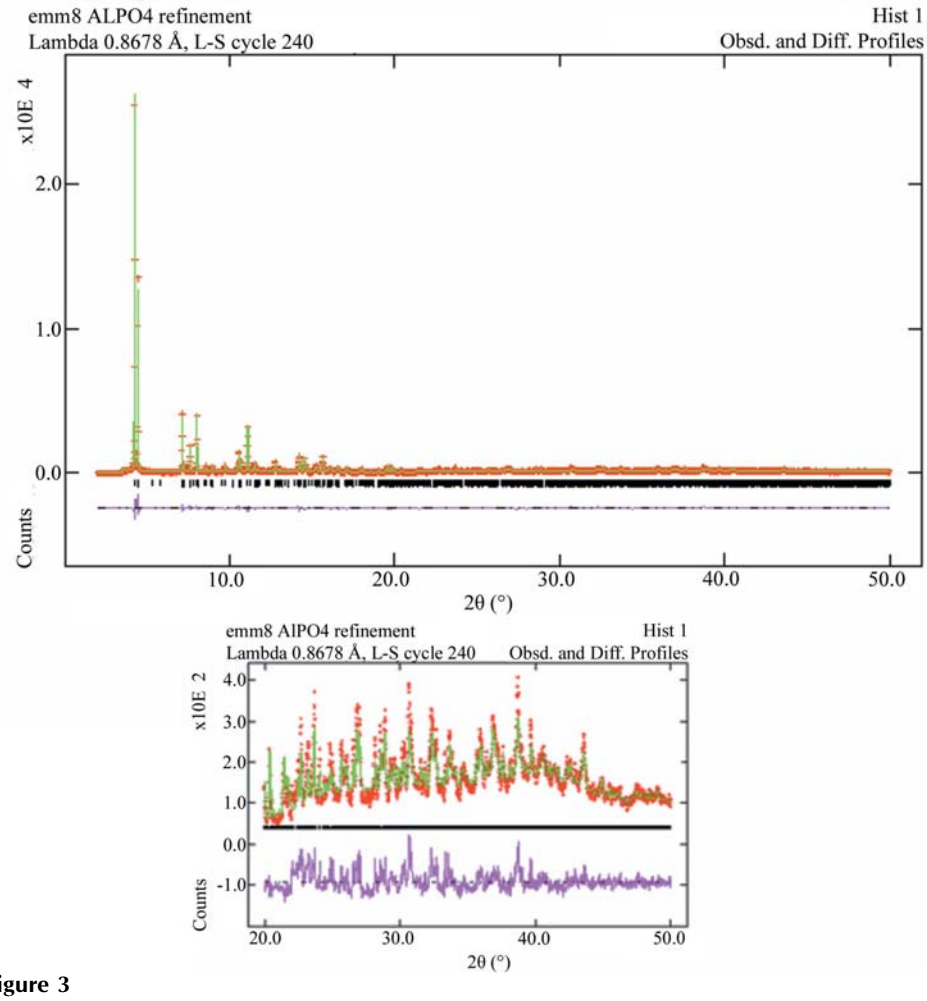

Figure 3
Match of the $AlPO_4$ model for EMM-8 to the powder diffraction pattern after Rietveld refinement.

hedral and penta-coordinated Al in the as-synthesized EMM-8 in a ratio of 1:1 and only T_d Al in the calcined material. ^{27}Al 3QMAS NMR shows a higher resolution revealing the presence of at least two types of T_d and penta-Al in the as-synthesized, and two distinct T_d species in the calcined EMM-8. The AlPO EMM-8 was made with fluorine in the gel and the combination of ^{27}Al and ^{19}F MAS along with ^{19}F $\rightarrow$ ^{27}Al CP/MAS data show that F is only coordinated to the penta-coordinated Al. The removal of F upon calcination results in a completely tetrahedral framework and only T_d Al. These NMR data, therefore, provided important constraints on the number of T atoms per unit cell and the connectivities of the T atoms. The detailed local structural information obtained by solid-state NMR helped guide the ultimate determination of the structure of AlPO EMM-8 using X-ray crystallographic techniques, as outlined above.

As mentioned above, after the completion of the Rietveld refinement, a preprint appeared announcing the structure of SSZ-51 (Morris *et al.*, 2004), a newly synthesized AlPO or SAPO, made with the same 4-dimethylaminopyridine as SDA used to create EMM-8. It is interesting to compare the results of the single-crystal determination made for SSZ-51 with the powder determination for EMM-8 reported in this work. In terms of framework geometry, it is clear that the accuracy of the structural determination is not greatly compromised by reliance on powder diffraction data. Ambiguities can exist, however, for the determination of unit-cell symmetry and unit-cell constants if only powder data are used. However, single-crystal electron diffraction techniques, even in a qualitative application, are very helpful for resolving such problems. As indicated in recent papers (Dorset *et al.*, 2005; Dorset *et al.*, 2006), the three-dimensional observation of the unit cell *via* electron diffraction is even more informative. Even though the electron-diffraction intensity data in Fig. 1 were not useful for structure determination, there are cases where zonal, as well as three-dimensional, determinations might be possible (Dorset *et al.*, 2005; Dorset *et al.*, 2007). The real difficulty with powder determinations is the unambiguous description of extra-framework species, since such models may not easily conform to a crystallographic description (Mortier & Bosmans, 1971; Mortier *et al.*, 1972). Even though very small crystals had been used for X-ray data collection from SSZ-51, there were enough resolved reflections to find the structure directing agent and some solvent sites. While single-crystal methods would certainly be

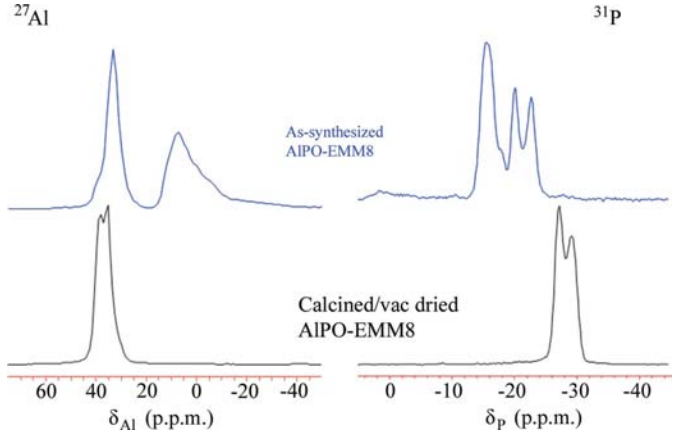

Figure 4
^{27}Al (left) and ^{31}P (right) MAS NMR of as-synthesized and calcined, vacuum-dried AlPO EMM-8.

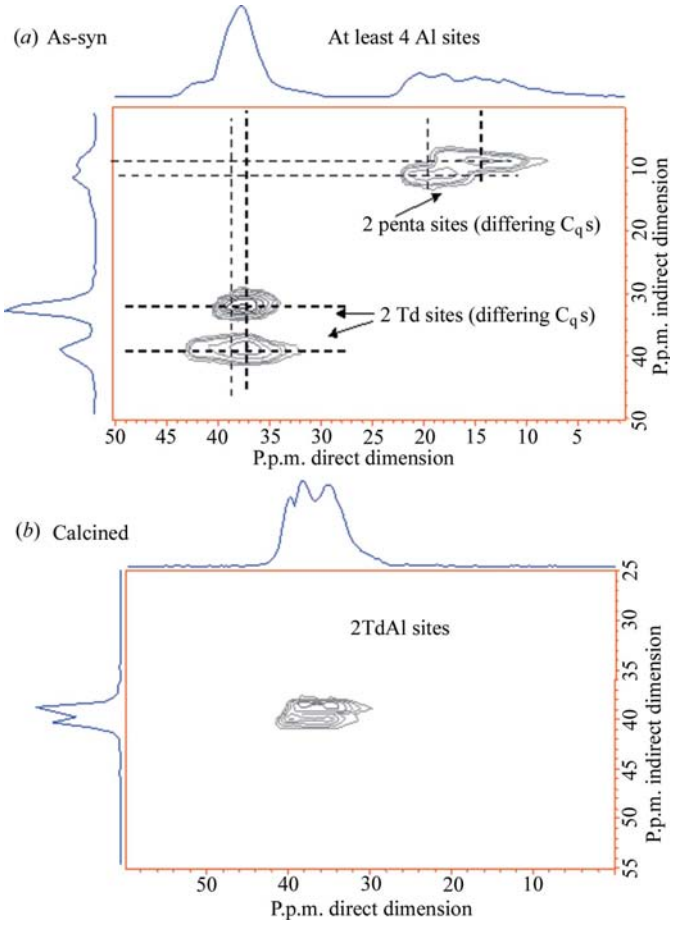

Figure 5
^{27}Al 3QMAS NMR spectra of as-synthesized and calcined, vacuum-dried AlPO EMM-8.

the favored choice when permitted, we have shown here that important additional information is available from complementary techniques.

The assistance of Matu Shah in the synthesis and of Boming Liang and Clarence Chase in recording NMR data is gratefully acknowledged. We are grateful to ExxonMobil Research and Engineering Co. for permission to publish this work.

References

Accelrys Inc. (1997). *Cerius*2. San Diego, USA.
Amoureux, J. P. & Pruski, M. (2002). *Encyclopedia of Nuclear Magnetic Resonance*, Vol. 9, pp. 226–251. New York: John Wiley and Sons.
Baerlocher, Ch., Hepp, A. & Meier, W. M. (1977). *Distance Least Squares Refinement Program, DLS*-76. ETH, Zürich.
Baerlocher, Ch., Meier, W. M. & Olson, D. H. (2001). *Atlas of Zeolite Framework Types*, 5th Revised Ed. Amsterdam: Elsevier (see also International Zeolite Association Structure Commission website: http://www.iza-structure.org for latest list of framework types).
Bell, R. G., Jackson, R. A. & Catlow, C. R. A. (1992). *Zeolites*, **12**, 870–871.
Burton, A. W. (2004). *Z. Kristallogr.* **219**, 866–880.
Corma, A. (2003). *J. Catal.* **216**, 298–312.
Dorset, D. L., Gilmore, C. J., Jorda, J. L. & Nicolopoulos, S. (2007). *Ultramicroscopy*. In the press.
Dorset, D. L., Kennedy, G. J., Strohmaier, K. G., Diaz-Cabanas, M. J., Rey, F. & Corma, A. (2006). *J. Am. Chem. Soc.* **128**, 8862–8867.
Dorset, D. L., Roth, W. J. & Gilmore, C. J. (2005). *Acta Cryst.* A**61**, 516–527.
Dumont, N., Gabelica, Z., Derouane, E. G. & McCusker, L. B. (1993). *Micropor. Mater.* **1**, 149–160.
Estermann, M. A., McCusker, L. B. & Baerlocher, Ch. (1992). *J. Appl. Cryst.* **25**, 539–543.
Fernandez, C., Amoureux, J. P., Chezeau, J. M., Delmotte, L. & Kesler, H. (1996). *Micropor. Mater.* **6**, 331–340.
Fernandez, C., Morais, C., Rocha, J. & Pruski, M. (2002). *Solid State Nucl. Magn. Reson.* **21**, 61–70.
Grosse-Kunstleve, R. W., McCusker, L. B. & Baerlocher, Ch. (1999). *J. Appl. Cryst.* **32**, 536–542.
Larson, A. C. & Von Dreele, R. B. (1994). *GSAS*. Los Alamos Laboratory, New Mexico, USA.
LeBail, A., Duroy, H. & Fourquet, J. L. (1988). *Mater. Sci. Bull.* **23**, 447–452.
Lok, B. M., Messina, C. A., Patton, R. L., Gajek, R. T., Cannan, T. R. & Flanigen, E. M. (1984). *J. Am. Chem. Soc.* **106**, 6092–6093.
Löwenstein, W. (1954). *Am. Miner.* **39**, 92–96.
Materials Data Inc. (2005). *JADE*. Materials Data Inc., Livermore, CA, USA.
McCusker, L. B. (1991). *Acta Cryst.* A**47**, 297–313.
McCusker, L. B. & Baerlocher, Ch. (1996). *Micropor. Mater.* **6**, 51–54.
Meier, W. M. & Moeck, H. J. (1979). *J. Solid State Chem.* **27**, 349–355.
Morris, R. E., Burton, A., Bull, L. M. & Zones, S. I. (2004). *Chem. Mater.* **16**, 2844–2851.
Mortier, W. J. & Bosmans, H. J. (1971). *J. Phys. Chem.* **75**, 3327–3334.
Mortier, W. J., Bosmans, H. J. & Uytterhoeven, J. B. (1972). *J. Phys. Chem.* **76**, 650–656.
O'Keeffe, M. & Hyde, S. T. (1997). *Zeolites*, **19**, 370–374.
Wagner, P., Nakagawa, Y., Lee, G. S., Davis, M. E., Elomari, S., Medrud, R. C. & Zones, S. I. (2000). *J. Am. Chem. Soc.* **122**, 263–273.
Wilson, S. T., Lok, B. T., Messina, C. A., Cannan, T. R. & Flanigen, E. M. (1982). *J. Am. Chem. Soc.* **104**, 1146–1147.